Evaluation of Z_{eff} Profile in Low-Density and High-T_{i} Discharges with Carbon Pellet Injection based on Space-Resolved EUV Spectroscopy in LHD*)

Xianli HUANG[1)], Shigeru MORITA[1,2)], Tetsutarou OISHI[1,2)], Motoshi GOTO[1,2)] and Hongming ZHANG[1)]

[1)]*Department of Fusion Science, Graduate University for Advanced Studies, Toki, Gifu 509-5292, Japan*
[2)]*National Institute for Fusion Science, Toki, Gifu 509-5292, Japan*

(Received 24 November 2014 / Accepted 26 February 2015)

Z_{eff} profile analysis has been carried out in a low-density and high-T_{i} discharge with carbon pellet injection. The evolution of the Z_{eff} profile shows a centrally peaked profile just after the pellet injection while the profile gradually returns to an original flat profile as a function of time. Comparison between the evolution of Z_{eff} and T_{i} profiles in the plasma center strongly suggests that there is a positive relation between Z_{eff} and T_{i}.

Keywords: Z_{eff} measurement, bremsstrahlung, EUV spectroscopy, high-T_{i}, carbon pellet

DOI: 10.1585/pfr.10.3402036

1. Introduction

Impurity behavior has been extensively studied in both theoretical and experimental fields in fusion research because impurities play an important role on the plasma performance [1, 2]. Impurity accumulation leads to a large radiation loss and ion dilution, especially in H-mode plasmas with a long impurity confinement time [3]. Recent experiments suggest an importance of the electron heating to avoid the impurity accumulation [4,5]. Gyro-kinetic and fluid simulations have been also used for understanding the impurity transport [6]. In the Large Helical Device (LHD), an improvement in plasma performance with increase in central T_{i} has been observed with carbon pellet injection [7]. It is therefore necessary to investigate the impurity behavior in such discharges.

The impurity content is commonly characterized by the effective ion charge $Z_{\mathrm{eff}} = \sum_{\mathrm{i}} n_{\mathrm{i}} Z_{\mathrm{i}}^2 / \sum_{\mathrm{i}} n_{\mathrm{i}} Z_{\mathrm{i}} = \sum_{\mathrm{i}} n_{\mathrm{i}} Z_{\mathrm{i}}^2 / n_{\mathrm{e}}$. Z_{eff} can be derived from the emissivity of bremsstrahlung, which is expressed by the following equation [8]:

$$\varepsilon_{\mathrm{brem}} = \frac{1.89 \times 10^{-28} n_{\mathrm{e}}^2 g_{\mathrm{ff}} Z_{\mathrm{eff}}}{T_{\mathrm{e}}^{1/2} \lambda^2} \exp\left(\frac{-12400}{T_{\mathrm{e}} \lambda}\right), \quad (1)$$

where $\varepsilon_{\mathrm{brem}}$ (W·cm^{-3}·Å), n_{e} (cm^{-3}), g_{ff}, T_{e} (eV) and λ (Å) stand for the emissivity, the electron density, the free-free gaunt factor, the electron temperature and the wavelength, respectively.

A Czerny–Turner spectrometer has been installed on the LHD to measure the radial bremsstrahlung profile in the visible range [9]. However, the visible bremsstrahlung profile is strongly affected and distorted by bremsstrahlung emission from the edge boundary of the LHD ergodic layer in low-density discharges [10]. As the electron density in high T_{i} discharges is usually below 2×10^{13} cm^{-3}, it becomes difficult to obtain Z_{eff} profiles using the visible spectrometer. On the contrary, the bremsstrahlung in the extreme ultraviolet (EUV) range is free of the non-uniform edge bremsstrahlung emission because of the higher photon energy in the EUV range compared with that in the visible range. In addition, the bremsstrahlung is much stronger in the EUV range. Therefore, Z_{eff} profiles in high-T_{i} discharges can be evaluated from the space-resolved measurement of EUV bremsstrahlung.

2. Experimental Setup

Two space-resolved EUV spectrometers have been installed on LHD [11, 12]. Both spectrometers include an entrance slit, a spatial-resolution slit, a varied-line-spacing holographic grating and a charge-coupled device (CCD) detector with 1024 × 255 pixels. Time resolution of the two systems was 200 ms in 2012 and has been improved to 50 ms after the installation of a new CCD for each system in 2013. The vertical spatial resolution of the systems is roughly 3 cm. A space-resolved spectrometer called "EUV-Short2" works in the wavelength range of 10 - 130 Å and can measure upper half of the elliptical plasma, as shown in Fig. 1. The other spectrometer, called "EUV-Long2", works in the wavelength range of 30 - 650 Å, which can measure either upper or lower half profile. A 0.5 μm-thick filter made of polyethylene terephthalate (PET) is installed in each system to reduce spike noises caused by high-energy NBI particles. The filter can effectively eliminate the spike noise. A spectrum measured by EUV-Long2 in a low density discharge is shown

author's e-mail: huang.xianli@nifs.ac.jp

*) This article is based on the presentation at the 24th International Toki Conference (ITC24).

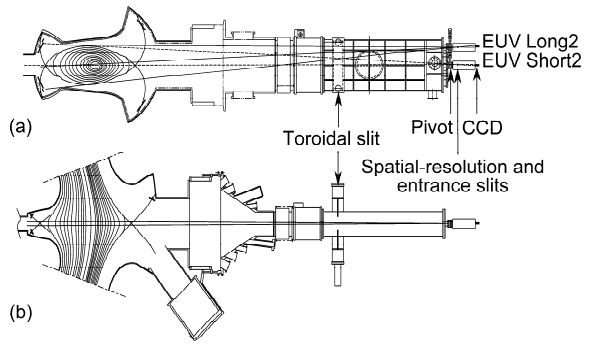

Fig. 1 (a) Side view and (b) top view of EUV systems on the LHD.

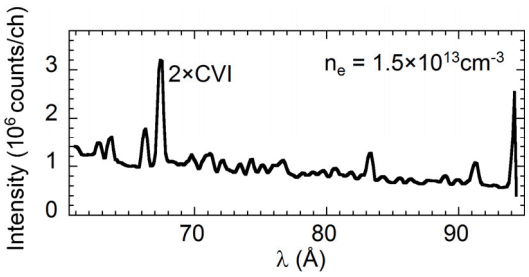

Fig. 2 EUV spectrum measured in a low-density discharge.

in Fig. 2. The continuum can be observed at the base line of the spectrum.

In order to obtain a better signal-to-noise ratio, the aperture sizes of the slits in the EUV systems are changed to 200 μm (width of entrance slit) × 2 mm (height of space-resolved slit), which is four and two times as large as the sizes of the usually used slits for EUV-Short2 and EUV-Long2, respectively. Consequently, new intensity calibration is necessary to obtain the absolute intensity. The EUV systems are calibrated by means of comparison between visible and EUV bremsstrahlung profiles. The visible bremsstrahlung profile has been measured by the above-mentioned Czerny–Turner spectrometer. Figure 3 shows the calibration results. Fitting with previous calibration curves are also plotted with solid lines. The calibration factor shows that the system brightness is enhanced by a factor of 4.0 and 2.2 for EUV-Short2 and EUV-Long2, respectively. This means the system brightness is approximately proportional to the size of the slit aperture.

3. Analysis of Z_{eff} Profile

A typical example of Z_{eff} profile analysis at λ = 77.4 Å - 80.0 Å is shown in Fig. 4. The vertical profile of the line-integrated signal is plotted in Fig. 4 (a) and radial profiles of n_e, T_e, ε and Z_{eff} are shown in Figs. 4 (b) - (e), respectively. The emissivity profile, ε, is derived from the line-integrated profile based on Abel inversion. The magnetic surface used in the inversion is calculated with VMEC code [13]. The emissivity near the last closed flux

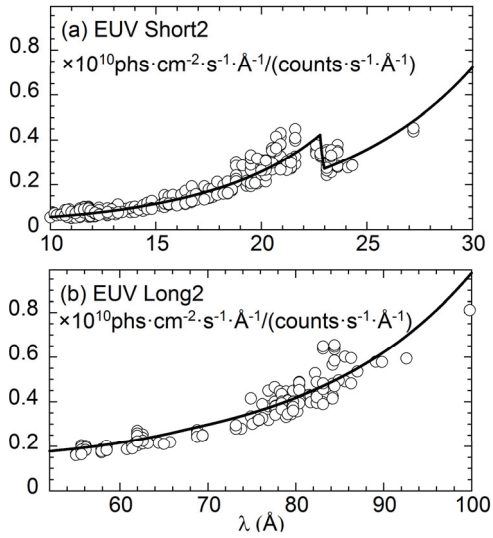

Fig. 3 Intensity calibration factors as a function of wavelength for (a) EUV Short2 and (b) EUV Long2. Solid lines denote fitting curves using previous calibration results.

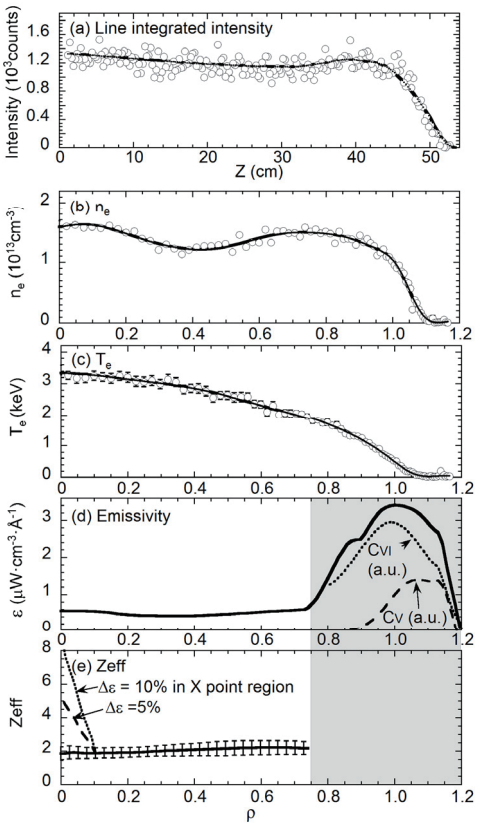

Fig. 4 (a) Line-integrated signal and radial profiles of (b) n_e, (c) T_e, (d) continuum emissivity at 77.4 Å - 80.0 Å and (e) Z_{eff}. Solid lines in (a) - (c) indicate curve fitting and shaded area in (d) and (e) denotes the region affected by recombination radiation. Dashed and dotted lines in (d) denote shapes of CV and CVI emissions. Dashed and dotted lines in (e) indicate Z_{eff} deviation assuming strong emissions from the X point region.

surface (LCFS) is much larger than that in the plasma core ($\rho < 0.75$) as seen in Fig. 4 (d). It seems that the large amount of continuum radiation is attributed to recombination radiation instead of bremsstrahlung because the intensity of bremsstrahlung is limited by $Z_{\rm eff}$, which should be less than 6 if the impurity density is determined by only carbon. Since the photon energy is around 158 eV, the recombination radiation mainly originates in C^{4+} and C^{5+}. This is verified by comparison of the edge continuum emissivity profile and the carbon line emissions, CVI 33.73 Å and Cv 40.27 Å + 40.73 Å, as shown in Fig. 4 (d). The line emission profiles reflect the distributions of corresponding ions. The edge emissivity profile seems to be a superposition of the shapes of the two line emission profiles. Despite the large amount of recombination radiation in the edge, the emissivity profile is basically free of recombination radiation in the plasma core ($\rho < 0.75$) because of the following reasons. First, the enhancement of continuum emissivity due to recombination radiation dramatically decreases with increasing electron temperature [14]. For instance, the enhancement factor of recombination radiation caused by C^{5+} is around 12 at $T_e = 0.2$ keV while the factor decreases to 1.2 at $T_e = 2$ keV. Second, the impurity ions contributing to the observed recombination radiation, namely, C^{4+} and C^{5+}, are mainly located in the edge. Therefore, the emission from the plasma core certainly consists of only the bremsstrahlung.

In order to complete the Abel inversion, the magnetic surface obtained with the VMEC code is linearly extrapolated to the region of $1 < \rho \leq 1.3$. If the bremsstrahlung continuum or impurity emissivity outside the LCFS is nonuniform in the poloidal direction, the measured line-integrated profile will be distorted. However, it is not the case in the EUV bremsstrahlung measurement because the energy is relatively high. The C^{4+} and C^{5+} ions distribute around the LCFS where the connection length L_c is still quite long, e.g., $L_c > 10^3$ m. Therefore, the ion density can be considered to be uniform in the poloidal direction and then the resultant recombination radiation with such ions will be also uniform. This is verified by an impurity simulation in the ergodic layer [15]. A possible uncertainty caused by the recombination radiation from X points of the ergodic layer should be also taken into account. Assuming that emissions from the X point region enhance the integrated emissivity outside the LCFS along a viewing chord of the spectrometer by a percentage of 5% or 10%, the $Z_{\rm eff}$ near plasma center increases abruptly, as shown in Fig. 4 (e). This effect is sometime observed in the measurement. Fortunately, the X point region with relatively strong emissions is usually narrow in the vertical direction, usually within $Z = \pm 5$ cm. Therefore, only the viewing chord passing through this narrow vertical region is affected by unnecessary emissions. It corresponds to the radial region of $\rho < 0.1$. In other words, the $Z_{\rm eff}$ profile can be always measured successfully in most radial ranges in the plasma core.

The error bars plotted in Fig. 4 (e) is calculated from the data scattering involved in the line-integrated intensity, the electron density and the electron temperature. The total uncertainty is estimated to be 20% - 30%.

4. Evolution of $Z_{\rm eff}$ Profile in High-T_i Discharges

Time evolution of the NBI port-through power $P_{\rm NBI}$, n_e, T_e, T_i, the plasma stored energy W_p and the radiation power $P_{\rm rad}$ are shown in Fig. 5. The $Z_{\rm eff}$ profile analysis is performed in six time frames, designated as F1-F6 as denoted in Fig. 5. A carbon pellet is injected at $t = 4.5$ s. The line-integrated density n_e increases from 1.0×10^{13} cm^{-3} to 2.2×10^{13} cm^{-3} after the pellet injection and then gradually decays to 1.4×10^{13} cm^{-3}. The electron temperature T_e is not significantly affected by the pellet. The ion temperature T_i increases from 3.1 keV to 4.2 keV and becomes higher than T_e after the injection (F2). The value of T_i is maintained at around 4.0 keV for 200 ms (F3). The decrease in T_i starts from $t = 5.0$ s and becomes lower than T_e after $t = 5.25$ s.

The radial profiles of $Z_{\rm eff}$, $n_{C^{5+}}/n_e$, T_i and T_e in the above-mentioned time frames F1-F6 are shown in Fig. 6. The $Z_{\rm eff}$ profile in Fig. 6 (a) is basically flat before the pellet injection. In the frame just after the injection (F2), the line-averaged $Z_{\rm eff}$ value increases by approximately 0.8 and a centrally peaked $Z_{\rm eff}$ profile occurs. At the same time, the T_i profile is increased as a whole and becomes higher than T_e in the central region ($\rho < 0.6$). All three profiles are maintained in the next time frame when the central T_i stays at 4.0 keV (F3). The normalized C^{5+} density ($n_{C^{5+}}/n_e$) pro-

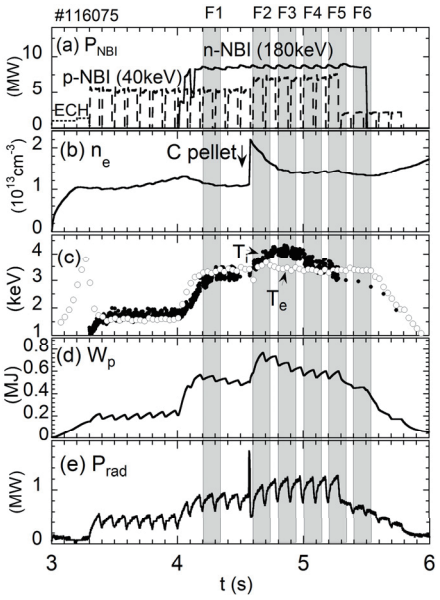

Fig. 5 Time evolution of (a) NBI port-through power, (b) n_e, (c) T_e and T_i, (d) plasma stored energy W_p and (e) radiation power $P_{\rm rad}$. Dashed areas indicate six time frames of F1-F6.

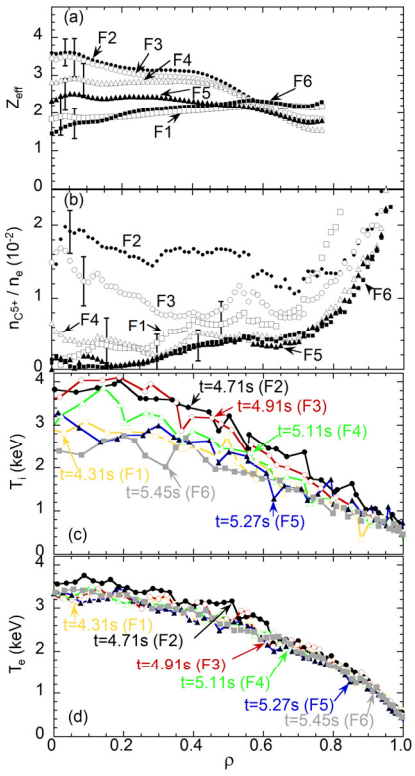

Fig. 6 Profiles of (a) $Z_{\rm eff}$, (b) $n_{\rm C^{5+}}/n_{\rm e}$, (c) $T_{\rm i}$ and (d) $T_{\rm e}$ in the six time frames of F1-F6.

file derived from CVI 28.5 Å is shown in Fig. 6 (b). The radial profile of C^{5+} density in the plasma core shows a good agreement with the $Z_{\rm eff}$ profiles in F2 and F3. The C^{6+} ion density is estimated to be roughly three to four times as high as the C^{5+} density just after the pellet injection by referring a result from similar discharges with carbon pellet injection. The central $Z_{\rm eff}$ is thus around 3.5. Taken into account the presence of other impurities, the $Z_{\rm eff}$ value should be slightly higher. Therefore, the present $Z_{\rm eff}$ value of 3.6 is quite reasonable in F2. When the $T_{\rm i}$ starts to decrease at t = 5.0 s, the $Z_{\rm eff}$ profile gradually returns to the original shape before the injection. Here, it is noted that the C^{5+} density profile measurement in the plasma core is not easy except for the period just after the pellet injection due to the low signal-to-noise ratio. The $T_{\rm i}$ profile tends to exhibit a similar behavior to the $Z_{\rm eff}$ profile. The $T_{\rm e}$ profile remains basically unchanged in all time frames.

Comparison between the $Z_{\rm eff}$ and $T_{\rm i}$ profiles strongly indicates that there is a positive relation between $Z_{\rm eff}$ and $T_{\rm i}$. Possible explanations are an enhancement of the absorption efficiency of NBI power and ion heating power per ion with increasing $Z_{\rm eff}$. It has been also identified that the plasma confinement is improved in such high $T_{\rm i}$ discharges with carbon pellet injection. A recent study shows there is a strong relation between the density of the carbon impurity and the thermal diffusivity [16]. The time behavior of the $Z_{\rm eff}$ and $T_{\rm i}$ profiles also suggests that $Z_{\rm eff}$ plays an important role in the confinement improvement.

5. Summary

The $Z_{\rm eff}$ profile has been successfully obtained in the plasma core ($\rho < 0.75$) from space-resolved profiles of bremsstrahlung in the EUV range. The recombination radiation can give a significant effect on the bremsstrahlung profile, in particular, in the edge region ($\rho > 0.75$) and also a small region ($\rho < 0.1$) near the plasma center. The time behavior of $Z_{\rm eff}$ profiles suggests a strong relation between $Z_{\rm eff}$ and $T_{\rm i}$.

Acknowledgments

The authors would like to thank all the members of the LHD experiment group for their cooperation including technical supports. This work was partially carried out under the LHD project financial support (NIFS14ULPP010) and also partly supported by the JSPS-NRF-NSFC A3 Foresight Program in the field of Plasma Physics (NSFC: No.11261140328, NRF: No.2012K2A2A6000443).

[1] T. Fülöp *et al.*, Phys. Plasmas **16**, 032306 (2009).
[2] G.P. Maddison *et al.*, Nucl. Fusion **43**, 49 (2003).
[3] C. Angioni *et al.*, Nucl. Fusion **54**, 083028 (2014).
[4] M. Valisa *et al.*, Nucl. Fusion **51**, 033002 (2011).
[5] M. Sertoli *et al.*, Plasma Phys. Control. Fusion **53**, 035024 (2011).
[6] N.T. Howard *et al.*, Plasma Phys. Control. Fusion **56**, 124004 (2014).
[7] S. Morita *et al.*, Plasma Sci. Technol. **13**, 290 (2011).
[8] H.Y. Zhou *et al.*, J. Appl. Phys. **107**, 053306 (2010).
[9] H.Y. Zhou *et al.*, Rev. Sci. Instrum. **79**, 10F536 (2008).
[10] H.Y. Zhou *et al.*, Rev. Sci. Instrum. **81**, 10D706 (2010).
[11] C.F. Dong *et al.*, Rev. Sci. Instrum. **81**, 033107 (2010).
[12] X.L. Huang *et al.*, Rev. Sci. Instrum. **85**, 043511 (2014).
[13] K. Yamazaki *et al.*, J. Plasma Fusion Res. **79**, 739 (2003).
[14] E.H. Silver *et al.*, Rev. Sci. Instrum. **53**, 1198 (1982).
[15] E.H. Wang, *Development of two-dimensional EUV spectroscopy for study of impurity behavior in ergodic layer of LHD* (The Graduate University for Advanced Studies, 2013) p.111-p.115.
[16] M. Osakabe *et al.*, Plasma Phys. Control. Fusion **56**, 095011 (2014).